npj | clean water

www.nature.com/npjcleanwater

ARTICLE OPEN

Surface decoration of bis-aminosilane cross-linked multiwall carbon nanotube ultrafiltration membrane for fast and efficient heavy metal removal

Ravi P. Pandey[1,2], Mariam Ouda[1,2], P. Abdul Rasheed[3], Fawzi Banat[1,2] and Shadi W. Hasan[1,2]✉

Heavy metals (HMs) are highly toxic water pollutants abundant in industrial wastewater. Herein, a bis[3-(trimethoxysilyl)propyl] amine (BTMSPA) cross-linked multiwalled carbon nanotube (MWCNT) nanomaterial (CQACNT) was synthesized by silanization of MWCNT-OH followed by grafting of positively charged quaternary ammonium groups (glycidyl trimethyl ammonium chloride (GTMAC)) by an epoxide ring-opening reaction. The composite membranes were prepared by the incorporation of CQACNT into the poly(ether sulfone) (PES) polymer matrix. The CQACNT-6 composite membrane exhibited a 3.5-fold increase in pure water permeability (PWP; 312.8 L m^{-2} h^{-1} bar^{-1}) as compared to the pristine PES (CQACNT-0) membrane (89.6 L m^{-2} h^{-1} bar^{-1}). Moreover, the CQACNT-6 composite membrane showed high HM removal rates (Pb: 89.53%; Ni: 90.42%; Cu: 91.43%; Zn: 91.86%) as compared to the CQACNT-0 membrane (Pb: 39.73%; Ni: 40.32%; Cu: 42.52%; and Zn: 43.91%). After 9 treatment cycles, the CQACNT-6 membrane retained up to 87%, and 94% of its initial PWP and initial Cu^{2+} rejection, respectively, compared to only 58%, and 54%, respectively for pristine CQACNT-0. The positively charged quaternary ammonium groups enhanced the surface features of PES and MWCNTS, resulting in competitive HM removal rates due to the electrostatic repulsion between the HM and the porous membranes, as well as high PWP.

npj Clean Water (2022)5:44 ; https://doi.org/10.1038/s41545-022-00189-8

INTRODUCTION

The global boom in industrialization has increased the level of toxic pollutants in various water bodies more than ever before[1,2]. Heavy metals (HMs) are persistent water pollutants with a toxic, non-biodegradable nature and a great tendency to accumulate in living organisms[3]. HMs are present as soluble salts in industrial wastewater, creating a threat to terrestrial fauna and aquatic life cycles[4]. HMs can decrease the oxygen intake of marine organisms, which causes severe injury to basic cellular processes, brain functions, kidneys, and liver[3]. Removing HMs from industrial wastewater is challenging due to their small size, diversity, and toxicity[5]. The most common HMs found in wastewater are Pb, Ni, Cu, and Zn[6,7]. Water remediation technologies such as ion exchange[8,9], adsorption[10], electrochemical treatment[3], chemical precipitation[7], coagulation and flocculation[1], and membrane filtration[11] have been applied for the removal of HM. The major drawbacks of ion exchange, adsorption, electrochemical treatment, chemical precipitation, coagulation and flocculation include operational and sludge disposal cost, partial removal of certain ions, and high energy consumption. Among all, membrane-based removal technologies have gained specific attention because they are considered environmentally friendly, cost-effective, and have a low-energy consumption[12–14]. Membrane composites applied in pressure-driven filtration processes can be divided into three categories based on their surficial charge (positively, negatively, and neutrally charged)[4,15]. Among all, positively charged membranes (PCMs) are highly effective in HM removal due to the electrostatic repulsion between the PCM surface and positively charged HMs, leading to enhanced separation efficiencies[4,7,12,14].

Recently, various studies have been conducted to prepare new PCMs for the removal of HMs[4,7,14,16–20]. Li et al. developed a type of PCM by surface grafting of polyamide with poly(amidoamine) dendrimer[4]. The prepared PCM exhibited more than 90% removal rates. A PCM prepared by self-assembly of ethylenediamine grafted multiwalled carbon nanotube (MWCNT) on the surface of polyethersulfone (PES) membrane showed a pure water flux (PWF) of 80.5 L m^{-2} h^{-1} at 10 bar pressure with a rejection rate of at least 90% for various HMs[14]. Zhou et al. developed a PCM by surface quaternization of poly (vinyl chloride *co* dimethylaminoethyl methacrylate), which exhibited 95% rejection of HMs and a pure water permeability (PWP) of 84 L m^{-2} h^{-1} bar^{-1} [7]. Wu et al. modified polyamide by surface-initiated atom transfer radical polymerization of methacryloxyethyltrimethyl ammonium chloride grafted to 2-bromoisobutyryl bromide[16]. The modified membrane exhibited a stable long-term operation for 168 h with more than 90% rejection of HMs and a PWF of 82.5 L m^{-2} h^{-1} at 6 bar applied pressure. Hyperbranched polyethyleneimine (PEI) cross-linked PCMs showed excellent performance for the removal of HMs[17,18]. Gong et al. synthesized a PCM by incorporating metal-organic frameworks into PEI and trimesic acid, showing a PWP of 12.2 L m^{-2} h^{-1} bar^{-1} and 90.9% rejection of $NiCl_2$[19]. A PCM prepared by interfacial polymerization of 1,2,3,4-cyclobutane tetracarboxylic acid chloride with PEI on a PES membrane exhibited a PWP of 156.85 L m^{-2} h^{-1} and a rejection of more than 90% for HMs[20]. These PCMs exhibited an excellent rejection rate for the HMs. However, the low PWP and poor long-term stability due to fouling are still major concerns[16,19,20]. Therefore, the development of PCMs with enhanced PWP and long-term stability can be driven by the incorporation of novel designed

[1]Center for Membranes and Advanced Water Technology (CMAT), Khalifa University of Science and Technology, PO Box 127788, Abu Dhabi, United Arab Emirates. [2]Department of Chemical Engineering, Khalifa University of Science and Technology, PO Box 127788, Abu Dhabi, United Arab Emirates. [3]Department of Biological Sciences and Engineering, Indian Institute of Technology Palakkad, Palakkad 678 557 Kerala, India. ✉email: shadi.hasan@ku.ac.ae

nanomaterials, such as MWCNTs, to attain boosted separation performances for the removal of HMs.

In this paper, a series of PCMs were fabricated by the surface silanization of hydroxyl MWCNT (MWCNT-OH) with bis[3-(trimethoxysilyl)propyl]amine (BTMSPA) followed by quaternization. To further enhance the positive charge, a glycidyltrimethylammonium chloride (GTMAC) was grafted on the surface of silanized MWCNT-OH by an epoxide ring-opening reaction. The performance of the developed PCMs was assessed in terms of PWP, HM rejection, antifouling behavior, as well as physicochemical properties. Moreover, a comparative analysis of the separation performance of the optimal PCM fabricated with reported PCMs in literature was carried out.

RESULTS AND DISCUSSION

Synthesis and characterization of CQACNT

The CQACNT was synthesized by a two-step reaction: (i) surface silanization process of MWCNT-OH by BTMSPA and (ii) epoxide ring-opening reaction of GTMAC to form CQACNT (Fig. 1(a)). The structural and surface morphology of the MWCNT-OH and CQACNT nanomaterials was assessed using the SEM images shown in Fig. 1(b)–(e). The MWCNT-OH shows a 1D tubular structure with a smooth surface (Fig. 1(c)). On the other hand, SEM analysis of CQACNT showed similarly a 1D tubular structure with linkages between tubes and rugged appearance ascribed to the crosslinking of MWCNT-OH by silanization (Fig. 1(e)). Further, TEM images (Fig. 1(f and g)) confirmed the 1D tubular structure of MWCNT-OH and CQACNT. The surface modification of MWCNT-OH by silanization followed by quaternization was confirmed by FT-IR spectra (Fig. 1(h)). The FT-IR spectrum of MWCNT-OH displays the bands at ~1705, ~1377 and ~1102 cm^{-1}, that are ascribed to the characteristic peaks for C=O, C–OH (bending) and C–O stretching, respectively. The MWCNT-OH mixture was crosslinked with BTMSPA to introduce silane and amine moieties on the surface. As compared to the FT-IR spectrum of MWCNT-OH, that of CQACNT showed two new peaks at 1180 cm^{-1}, and 1022 cm^{-1} corresponding to the absorption band for C–N and Si–O–C. This confirmed the successful grafting of the silane and amine moiety onto the surface of MWCNT-OH. Furthermore, a new peak at 1484 cm^{-1} corresponding to C–N^+ confirmed the grafting of the quaternary ammonium groups. These observations confirm that silanization followed by quaternization of MWCNT-OH have been successfully carried out. MWCNT-OH is a graphitized nanomaterial that has equivalent elemental domains of the parallel stacking of hexagonal carbon structure. The XRD pattern was used to recognize structural modification after reaction with BTMSPA. Figure 1(i) shows the XRD patterns of the MWCNT-OH and CQACNT nanomaterials. XRD patterns of MWCNT-OH showed characteristic peaks at 2θ of 26.18° (002), 43.4° (100), 53.1° (004), and 78.8° (110)[21]. After modification, the XRD patterns of CQACNT showed that the peak positions remained unchanged with a decrease in the intensity, demonstrating the silanization and functionalization occurring on the surface of MWCNT-OH.

XPS analysis was used to determine the surface atomic contents of the MWCNT-OH and CQACNT. The XPS survey spectrum of MWCNT-OH confirmed the presence of C 1 *s*, and O 1 s at binding energies (B.E.) of 283.7 eV, and 532.6 eV, respectively, while CQACNT shows Si 2*p*, Si 2 *s*, C 1 *s*, N 1 *s*, and O 1 *s* at the B.E. of 102 eV, 152 eV, 283.7 eV, 401 eV, and 532.6 eV, respectively (Supplementary Fig. 1). It can be seen that the survey spectrum of CQACNT showed two new peaks of N 1 *s*, and Si 2*p*, and confirmed the successful silanization and functionalization of the MWCNT-OH. The deconvolution of the bands in the C 1 *s*, O1*s*, Si 2*p*, and N 1 *s* high-resolution XPS (HR-XPS) spectra of MWCNT-OH and CQACNT is shown in Fig. 2(a)–(d). The C 1*s* HR-XPS spectra of MWCNT-OH and CQACNT could be deconvoluted into three major bands at B.E. of 284.5 eV, 285.6 eV, and 286.5 eV, assigned to the graphitic structure (C=C), C–C (Sp^3) defect bonds on the MWCNT-OH structure, and C–O bonds in alcohols, phenols, and ethers, respectively[22]. It can be seen that the band at B.E. of 286.5 eV in CQACNT became intense and broad, which could be attributed to the overlaps of B.E. of the C–N bond with the C–O[23]. The deconvoluted O1*s* HR-XPS spectrum of MWCNT-OH shows three peaks at B.E. of 531.8 eV, 533.1 eV, and 535.2 eV, attributed to the O=C from quinone, O–C from alcohol and phenol, and O–H from water, respectively[22]. As compared to the deconvoluted O 1 *s* HR-XPS spectrum of CQACNT with MWCNT-OH, two new broad bands in CQACNT were observed at B.E. of 532.5 eV, and 534 eV, assigned to –O_xSi overlapped with parental O=C and O–C bands and Si–OH or Si–O–Si band, respectively (Fig. 2(b))[24]. The deconvoluted Si 2*p* HR-XPS spectrum of CQACNT, showed broad bands at B.E. of 102.8 eV, and 104 eV, assigned to Si-O bonded to MWCNT-OH and Si-O-Si and confirmed the successful grafting of BTMSPA. Furthermore, the HR-XPS spectrum of N 1 *s* of CQACNT showed two peaks at the B.E. of 400.7 eV, and 402 eV, assigned to N-C to amine, and N^+-C to positively charged quaternary ammonium groups, respectively (Fig. 2(d)).

Membrane preparation and characterization

The CQACNT composite membranes were prepared by NIPS using a dope solution of CQACNT (0–8 wt%) with PES. The detailed membrane fabrication process, the chemical structure of the membrane, the possible interactions between PES and the CQACNT, and optical images are given in Fig. 3(a). It is expected that the CQACNT is stabilized in the PES matrix by forming a strong H-bond between the oxygen-containing groups. The optical images of the pristine CQACNT-0 and modified membrane CQACNT-6 display white and dark colors, respectively. Figure 3(b) shows the FT-IR spectra of the CQACNT-0 membrane and the CQACNT-6 composite membrane. The absorption bands at ~1574 cm^{-1}, 1395 cm^{-1}, 1236 cm^{-1}, and 1147 cm^{-1} are attributed to the stretching vibrations of aromatic C=C, C–H, symmetric S=O and asymmetric S=O, respectively, from PES moieties[25]. The presence of silica moieties (silanization) in the CQACNT-6 membrane was confirmed by an absorption band at ~1072 cm^{-1} attributed to the stretching vibration of Si–O–C group. Furthermore, the functionalization of the CQACNT-6 membrane with quaternary ammonium groups was confirmed by the presence of absorption bands at ~1485 cm^{-1}, and 1180 cm^{-1} levels attributed to the C–N^+ and C–N stretching, respectively. Due to the very low concentration of the CQACNT nanomaterial (6 wt%) in PES polymer matrix, the intensities of a few peaks are either weak or merged with other peaks. XRD was used to recognize the possible structural changes within the membrane matrix. Figure 3(c) shows the XRD patterns of CQACNT-0, and the CQACNT-6 membrane. The CQACNT-0 membrane showed a characteristic diffractogram of an amorphous membrane that has a maximum intensity peak at about 2θ value of 17.87° and a minor peak at about 2θ value of 43.33°. Interestingly, the XRD pattern of the CQACNT-6 membrane exhibited an amorphous nature where the characteristic PES 2θ peaks were still detected but wider with a higher peak intensity and shifted from 17.87° to 18.90°. The broadening and shifting of the peak at 18.90° can be attributed to the incorporation of the CQACNT nanomaterial into PES.

The structural morphology (top, bottom, and cross-sectional surfaces) of the CQACNT- (0-6), MWCNT-OH-6, and CASCNT-6 membranes were studied using SEM (Fig. 4). SEM images of the top surfaces of all membranes revealed a smooth, dense structure, free from any defects. However, the SEM image of the bottom surface of membranes displayed a visible distribution of the pores. The density and size of the pores on the bottom surface increase with the incorporation of CQACNT. Cross-sectional SEM images of

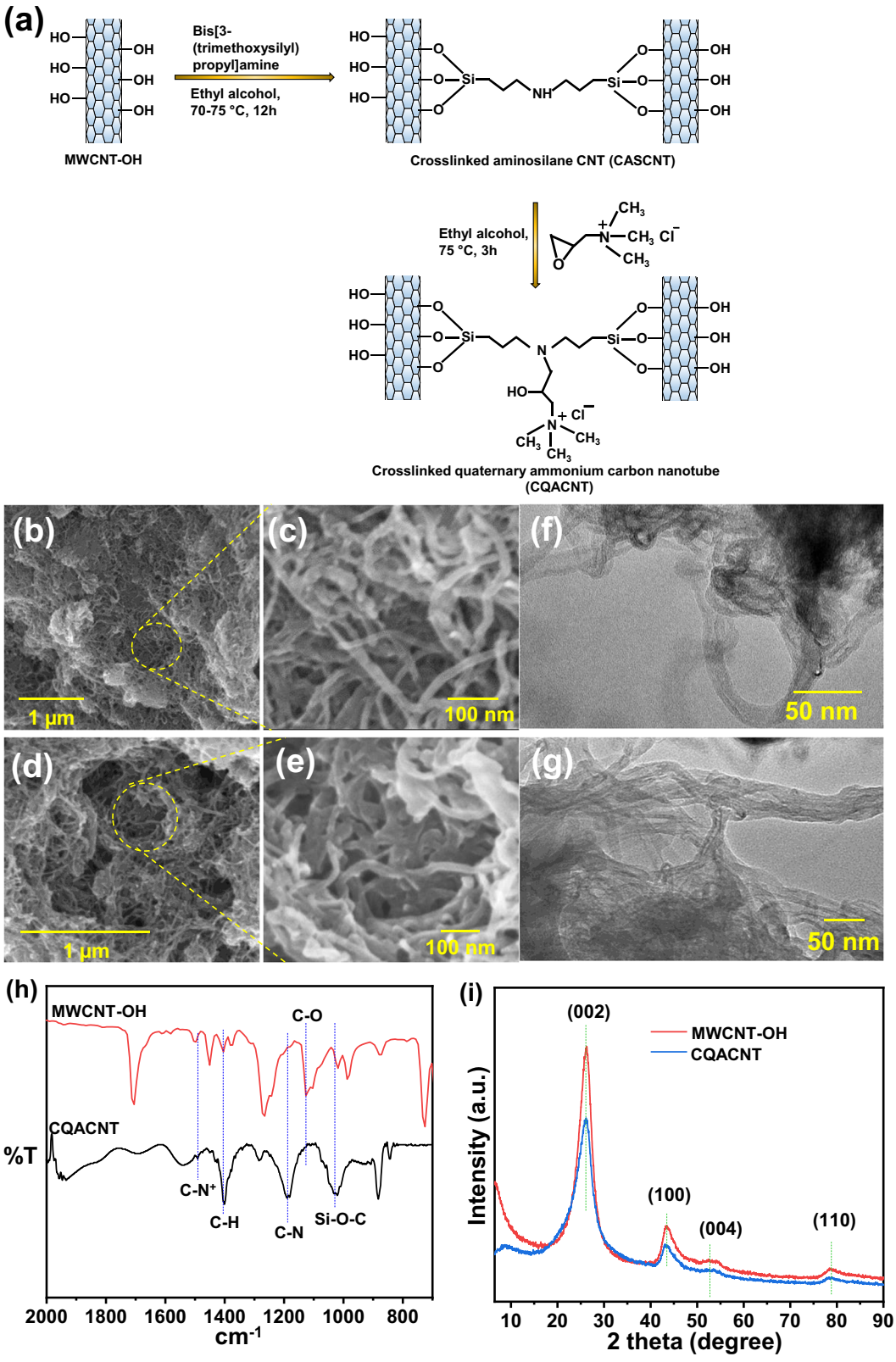

Fig. 1 Synthesis and morphological and spectroscopic studies of cross-linked quaternary ammonium carbon nanotube (CQACNT). **a** Schematic reaction route for the synthesis of CQACNT; **b** SEM image of MWCNT-OH; **c** high-resolution SEM image of MWCNT-OH; **d** SEM image of CQACNT; **e** high-resolution SEM image of CQACNT; **f** TEM image of MWCNT-OH; **g** TEM image of CQACNT; **h** FT-IR spectra of MWCNT-OH and CQACNT; **i** XRD pattern of MWCNT-OH and CQACNT.

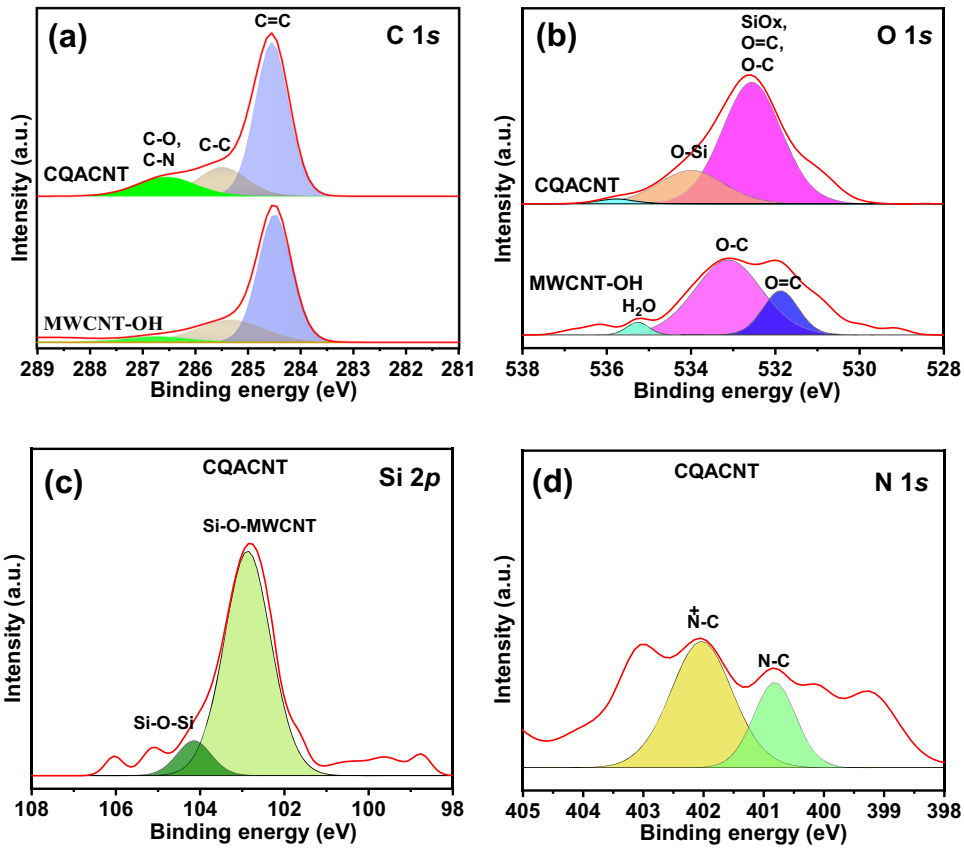

Fig. 2 High-resolution XPS spectra of MWCNT-OH and CQACNT. a C 1*s*; **b** O 1*s*; **c** Si 2*p*; **d** N 1*s*.

the prepared membranes showed a sponge-like structure with asymmetric fingers and a dense top layer. Incorporation of the CQACNT into the PES membrane matrix caused an increase in the porous structure with irregular fingers, attributed to the silanization and functionalization with quaternary ammonium groups.

The roughness of a membrane surface plays a crucial role in determining the separation performance and the fouling tendency of a membrane. A membrane with a rougher surface has a higher tendency to foul, thus declining the separation performance with time[26]. Figure 5(a)–(g) shows the AFM analysis of the CQACNT-0 and CQACNT-6 composite membrane. The AFM images confirmed the decrease in the surface roughness after the addition of CQACNT to the PES matrix. The results showed actual surface area roughness (R_a) and root means square roughness (R_q) of 59.7 nm, and 72.2 nm, respectively for CQACNT-0 and 25.1 nm, and 31.1 nm, respectively for CQACNT-6 (Fig. 5(g)). This could be attributed to the migration of the functionalized CQACNT nanomaterial to the membrane interface during the NIPS phenomenon, creating a more hydrophilic surface area that ultimately results in a smoother surface.

Membrane wettability, surface free energy, and WU are crucial properties that regulate its separation performance in dynamic filtration systems. The measure of the WCA was used to determine the wettability of the membrane[27]. A low value of WCA designates that the membrane surface is highly wetted, leading to enhanced water permeation and anti-fouling capacity[28]. Figure 6(a) and (b) show the static and dynamic WCA of the prepared CQACNT-(0-6), MWCNT-OH-6, and CASCNT-6 composite membranes. The static WCA of the CQACNT composite membranes decreased with the increased incorporation of CQACNT into PES. CQACNT-6 showed the lowest static WCA (46°), which is 1.51-fold, 1.35-fold, and 1.34-fold less, as compared to the pristine CQACNT-0, MWCNT-OH-6, and CASCNT-6 membranes, respectively. The dynamic WCA of the prepared membranes showed a decrease with time. The CQACNT-6 membrane showed the highest drop in dynamic WCA (15°; from 46° to 31°, over a period of 160 s), as compared to the pristine CQACNT-0 (6°), MWCNT-OH-6 (9°), and CASCNT-6 (9°) membranes (Fig. 6(b)), demonstrating enhancement in the overall wettability. The increased wettability of the CQACNT-6 membrane is attributed to the exceptional hydrophilic nature of the CQACNT. Furthermore, the wettability of the prepared membranes was evaluated by calculating the membrane-water interfacial free energy $(-\Delta G_{SL})$ (Fig. 6(c)). A high value of $-\Delta G_{SL}$, represented a more wetted membrane surface and thus excellent affinity for water[29]. The CQACNT-6 membrane showed the highest $-\Delta G_{SL}$ (131.88 mJ m^{-2}), as compared to the pristine CQACNT-0 (108.73 mJ m^{-2}), MWCNT-OH-6 (116.14 mJ m^{-2}), and CASCNT-6 (117.42 mJ m^{-2}) membranes, indicating the high wettability of the CASCNT-6 membrane. The water holding capacity in the membrane matrix provides an indication of the unobstructed pathway for water permeation during the dynamic filtration process. The water holding capacity of each membrane was evaluated in terms of WU (Fig. 6(d)). The amount of water content present in the membrane matrix depends on the ionic clusters, wettability, and void volumes existing in the membrane matrix[30]. The WU was found to increase upon blending of CQACNT into the PES matrix. The CQACNT-6 membrane exhibited a higher WU (107.53%), as compared to the pristine CQACNT-0 WU (59.42%).

Surface charge, IEC, porosity, and MPS analysis of prepared membranes

The surface zeta potential of a membrane is a vital property that expressly affects the rejection capability of charged pollutants. The surface zeta potential of the membranes developed was estimated in water for a wide pH range (4–9) and is presented in Fig. 7(a). The zeta potential of the pristine CQACNT-0 membrane

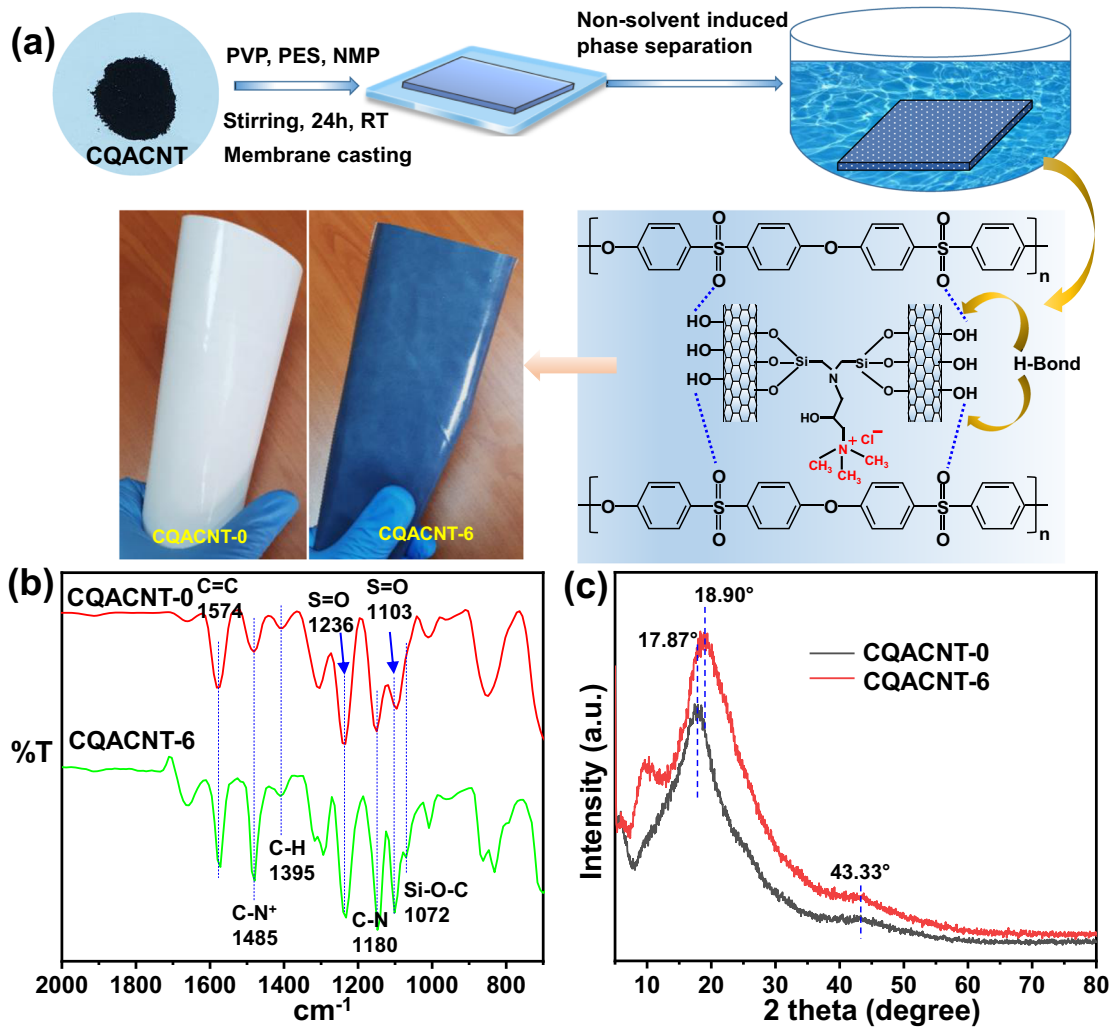

Fig. 3 Membrane fabrication and chemical characterization. a Membrane fabrication process, chemical structure of the membrane, possible interactions between PES and CQACNT, and optical images of the pristine CQACNT-0 and CQACNT-6 membranes; **b** FT-IR spectra of the CQACNT-0 and CQACNT-6 membranes; **c** Powder XRD patterns of the CQACNT-0 and CQACNT-6 membranes.

was ~−9.38 mV, which was transformed to a positively charged surface after the incorporation of CQACNT. The CQACNT-6 membrane showed a charge of +20.46 mV at pH = 6. It can be seen that the MWCNT-OH and CASCNT incorporated membranes, namely MWCNT-OH-6, and CASCNT-6 exhibited negatively charged surfaces with zeta values of −6.38 mV, and −5.23 mV at pH = 6, respectively. The incorporation of quaternized CQACNT into the PES polymer matrix resulted in a stronger positively charged surface, which indicates that many positively charged quaternary ammonium groups occur on the membrane surface. The positively charged surface will efficiently boost the strong positive-positive electrostatic repulsion between the CQACNT composite membranes and positively charged pollutants. Furthermore, the presence of a positively charged surface of developed CQACNT membranes was confirmed by IEC. The IEC represents the sum of all positively charged active sites or quaternary ammonium groups that are responsible for the exchange of ions in the membrane matrix. It can be seen that the IEC of the pristine CQACNT-0 membrane increased with the incorporation of CQACNT, and the CQACNT-6 composite membrane showed a maximum IEC of 0.71 meq g^{-1} (Supplementary Fig. 2).

Membrane porosity and MPS are crucial properties that significantly influence water permeability and HM rejection capability. These properties are functions of the ionic clustering of quaternary ammonium groups and membrane-water affinity. The porosity and MPS of the membranes developed are given in Fig. 7(b). It can be seen that the porosity and MPS increased upon the incorporation of CQACNT into PES. The CQACNT-6 composite membrane showed high porosity and MPS (porosity = 69.61%; MPS = 44.1 nm) as compared to the pristine CQACNT-0 (porosity = 57.72%; MPS = 27.5 nm), MWCNT-OH-6 (porosity = 64.18%; MPS = 33.9 nm), and CASCNT-6 (porosity = 62.42%; MPS = 32.9 nm) membranes. This trend can be explained by the increase in membrane wettability as a result of CQACNT. This leads to a faster exchange rate between solvent (NMP) and non-solvent (DI water), creating a more porous structure[31]. Furthermore, the quaternary ammonium groups existing in the CQACNT made ionic clusters that provided additional affinity toward water, consequently enhancing the porosity of the membrane.

PWP and heavy metal ion removal efficiency

The PWP of the CQACNT composite membranes increased remarkably by incorporating CQACNT into PES (Fig. 8(a)). The CQACNT-6 composite membrane exhibited a 3.5-fold increase in PWP (312.8 L m^{-2} h^{-1} bar^{-1}) as compared to the pristine CQACNT-0 membrane (89.6 L m^{-2} h^{-1} bar^{-1}). It can be seen that as compared to PES membranes incorporated with MWCNT-OH and

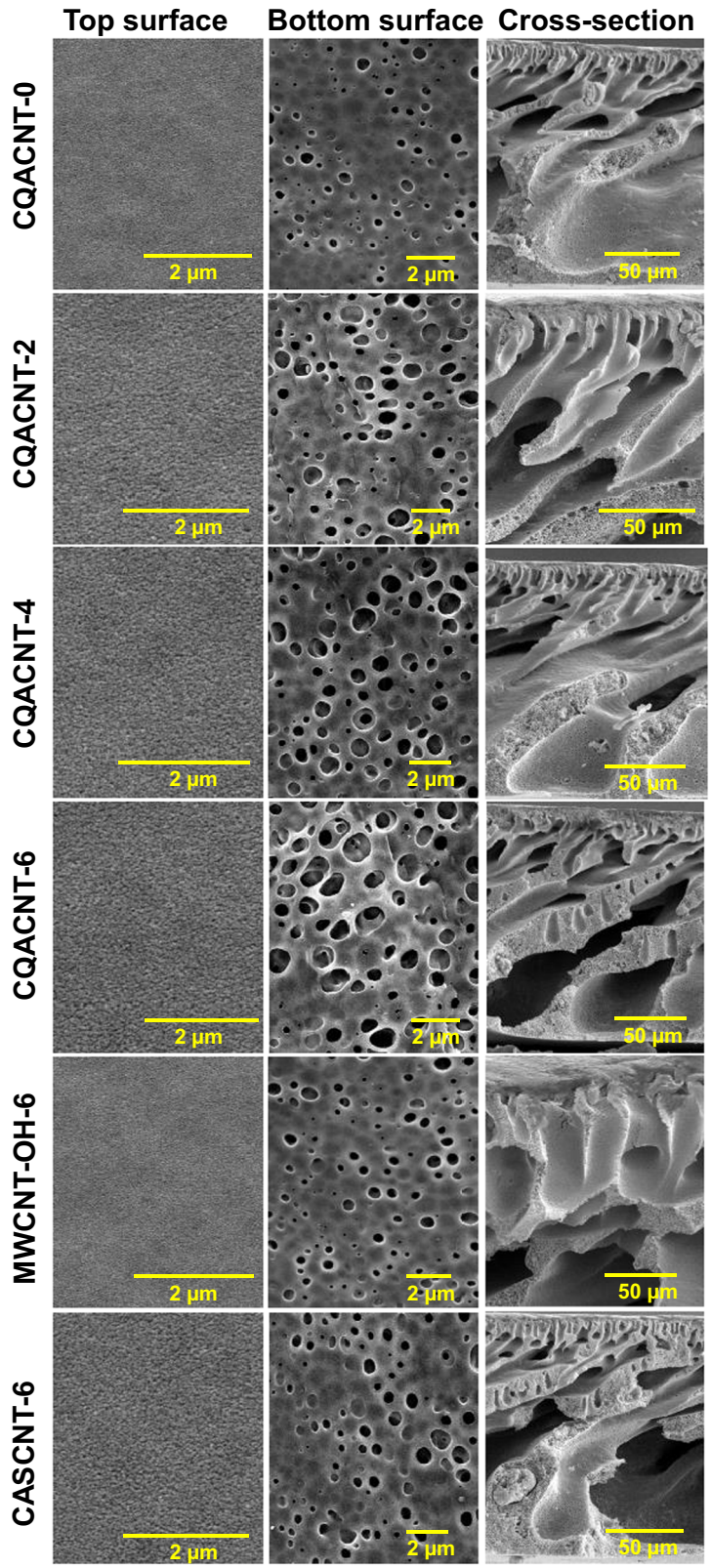

Fig. 4 Structural morphology of fabricated membranes. SEM micrographs of CQACNT (0-6), MWCNT-OH-6, and CASCNT-6 membranes: top surface, bottom surface and cross section.

CASCNT (MWCNT-OH-6 and CASCNT-6), the CQACNT modified membrane (CQACNT-6) showed a 1.9-fold, and 2.15-fold increase in PWP, respectively. This could be attributed to the creation of additional water pathways by the ionic functionalities present in CQACNT. These results show trends similar to what was observed in WU, IEC, porosity, and wettability of the developed membranes.

Figure 8(b) shows a schematic representation of the electrostatic repulsion mechanism between the positively charged

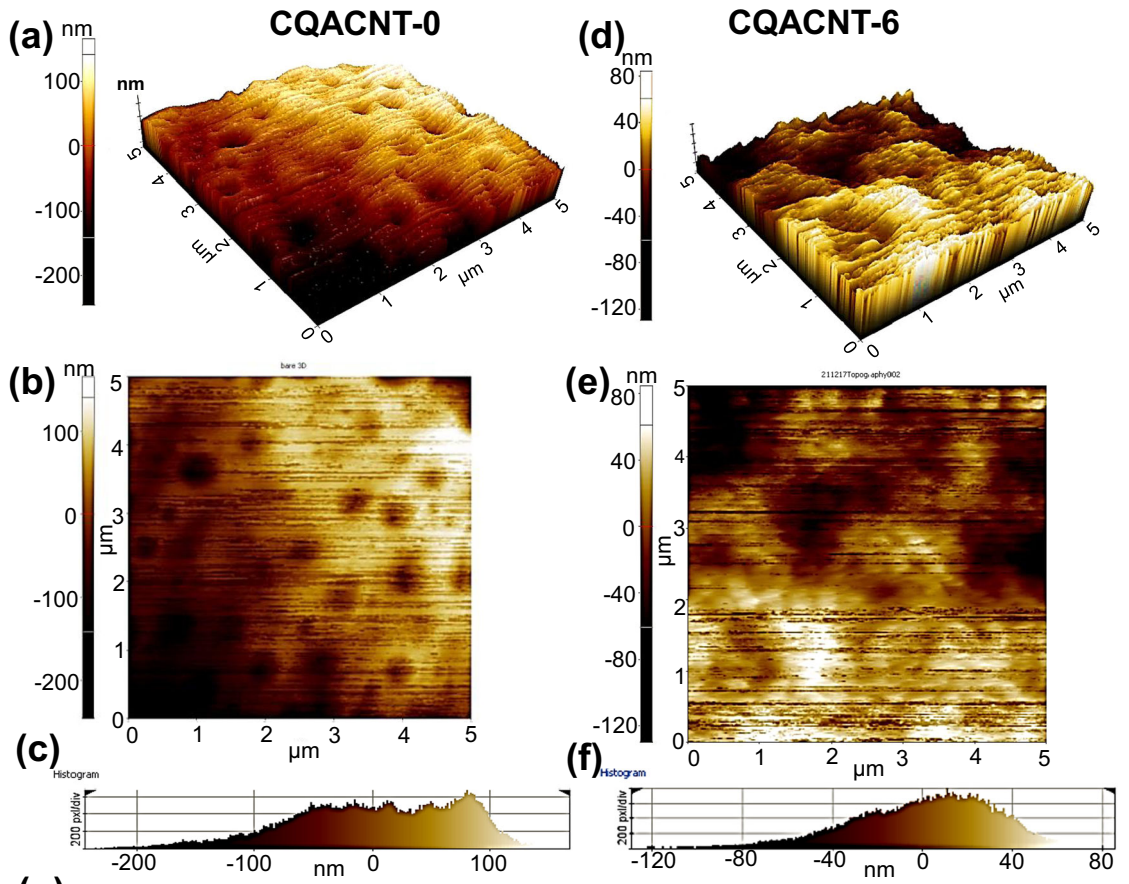

Membrane	Min(nm)	Max(nm)	Mid(nm)	Rpv(nm)	Rq(nm)	Ra(nm)	Rz(nm)	Rsk	Rku
CQACNT-0	-245.948	166.081	-39.934	412.028	72.197	59.699	404.829	0.410	2.645
CQACNT-6	-130.025	84.658	-22.683	214.682	31.122	25.079	206.544	0.441	3.004

Fig. 5 AFM images of fabricated membranes. a 3D image of CQACNT-0 membrane; **b** 2D image of CQACNT-0 membrane; **c** Histogram of CQACNT-0 membrane; **d** 3D image of CQACNT-6 membrane; **e** 2D image of CQACNT-6 membrane; **f** Histogram of CQACNT-6 membrane; **g** Surface roughness of CQACNT-0 and CQACNT-6 membranes.

surface of the CQACNT composite membrane and metal ions during separation. It is expected that the highly positively charged surface of CQACNT composite membrane repels the positively charged metal ions, thus helping in improving the separation performance. The rejection efficiency of the fabricated membranes was evaluated by ultrafiltration of different heavy metal ions (Fig. 8(c)). The rejection of CQACNT composite membranes increased with the CQACNT content in the membrane matrix, and CQACNT-6 showed high rejection values (Pb: 89.53%; Ni: 90.42%; Cu: 91.43%; Zn: 91.86%) in comparison with CQACNT-0 (Pb: 39.73%; Ni: 40.32%; Cu: 42.52%; Zn: 43.91%). Furthermore, CQACNT-6 exhibited a 1.78-fold and 1.96-fold increase in Zn^{2+} rejection values as compared to the MWCNT-OH-6 and CASCNT-6 composite membranes, respectively. The high rejection performance of the CQACNT-6 membrane is attributed to a very high electrostatic repulsion (Donnan exclusion) between the surface of the PCM and metal ions. All membranes showed similar rejection patterns, with minor differences attributed to the steric hindrance of different ions ($Pb^{2+} < Ni^{2+} < Cu^{2+} < Zn^{2+}$). The steric hindrance increases with the hydration radius of the metal ion, thus increasing rejection. In this case, Zn^{2+} showed the highest hydration radius (4.30 Å), while Pb^{2+} was the lowest (4.01 Å) among all metal ions[14]. Thus, for the developed CQACNT composite membranes, it may be conjectured that electrostatic repulsion and steric hindrance are jointly played for attaining high rejection for heavy metals.

The effects of applied pressure and feed concentration on the separation performance of the CQACNT-0 and CQACNT-6 composite membranes were evaluated (Fig. 8(d) & Supplementary Fig. 3). It can be seen that as the applied filtration pressure and concentration of metal ions increase, the rejection efficiency for both membranes decreases. The CQACNT-6 composite membrane showed a smaller drop in Zn^{2+} removal efficiency upon increasing the applied pressure from 1 bar to 4 bar (8.22%), as compared to CQACNT-0 (29.2%). A similar trend was observed in the feed concentration, where the Zn^{2+} removal efficiency decreased by 7.69% for CQACNT-6 and by 22.3% for CQACNT-0 when the feed concentration from 20 ppm to 100 ppm. The separation performances of the CQACNT-6 composite membrane in terms of PWP and HM removal were as compared to the reported literature on MWCNT porous membranes (Table 1). The CQACNT-6 composite membrane exhibited excellent PWP with competitive HM removal efficiency as compared to similar studies.

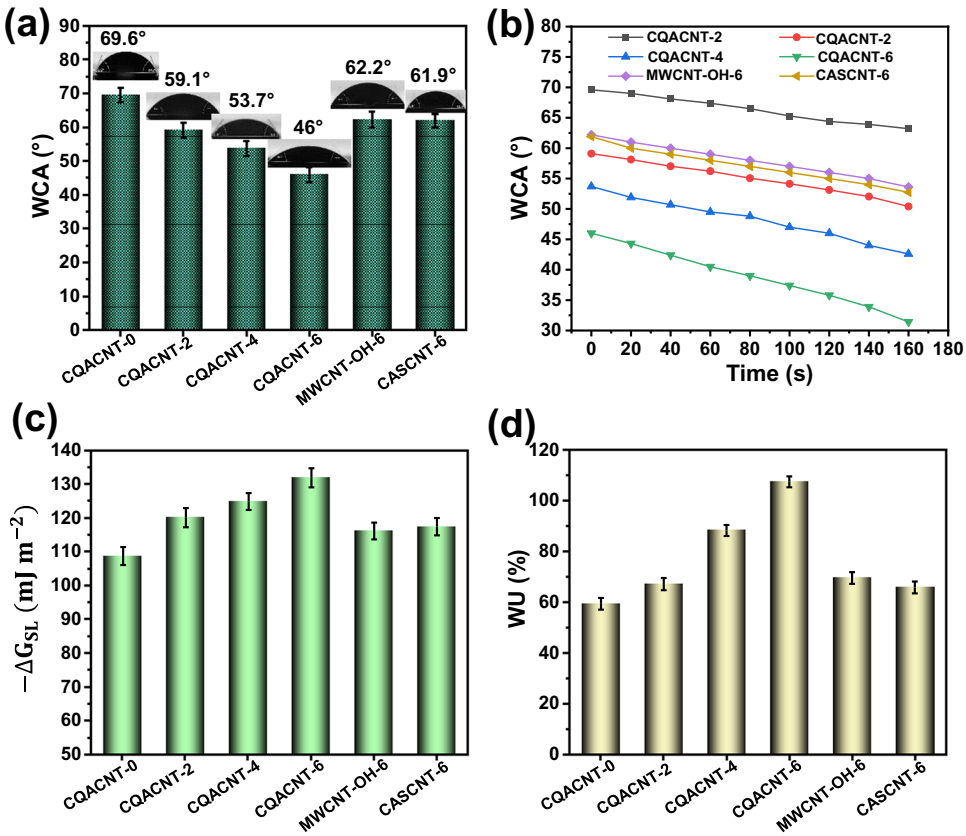

Fig. 6 Wettability and water uptake of pristine and composite membranes. a Static water contact angle; **b** Dynamic water contact angle; **c** Surface free energy of CQACNT, MWCNT-OH, and CASCNT composite membranes; **d** Water uptake of CQACNT, MWCNT-OH, and CASCNT composite membranes. Error bars represent the standard deviation between three reported values.

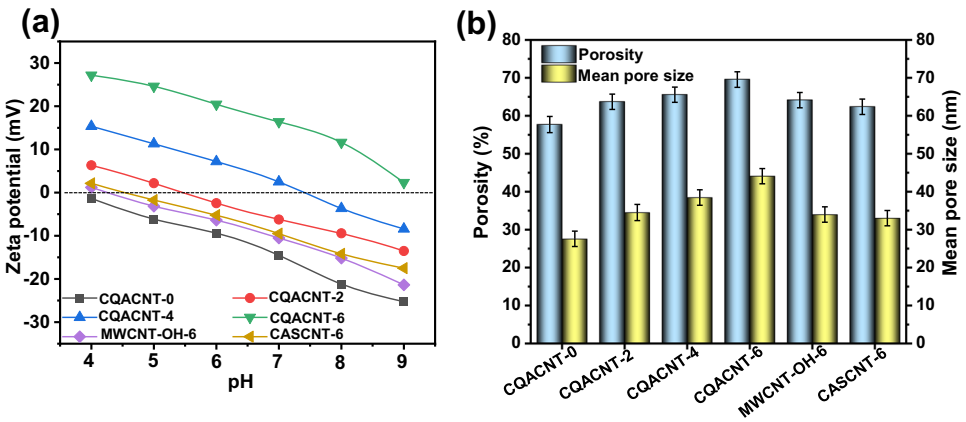

Fig. 7 Surface charge and pore characteristics of CQACNT, MWCNT-OH, and CASCNT composite membranes. a Zeta potential; **b** Porosity and mean pore size. Error bars represent the standard deviation between three reported values.

Anti-fouling and long-term durability test

The antifouling behavior of the CQACNT, MWCNT-OH-6, and CASCNT-6 composite membranes against metal ions (Pb^{2+}, Ni^{2+}, Cu^{2+}, and Zn^{2+}) was estimated in terms of HM adsorption. High adsorption leads to higher chances of blocking the membrane pores by forming a concentrated layer, decreasing the antifouling capacity. The amount of metal ions adsorbed on the developed composite membranes is shown in Fig. 9(a). It can be seen that the adsorption capacity decreased with increasing CQACNT content. Among all membranes developed, the CQACNT-6 membrane showed the lowest adsorbed amount for Pb^{2+} (4.21 μg cm^{-2}), Ni^{2+} (5.4 μg cm^{-2}), Cu^{2+} (6.42 μg cm^{-2}), and Zn^{2+} (7.61 μg cm^{-2}). The CQACNT-6 membrane showed 9-times, 11-times, and 10-times lower adsorption capacity of Pb^{2+}, as compared to the pristine CQACNT-0, MWCNT-OH-6 and CASCNT-6 membranes, respectively. The decrease in the HM adsorption is attributed to the increased positive charge by incorporating CQACNT. The electrostatic repulsion produced between the positively charged surface of the CQACNT-6 membrane and positively charged HM ions leads to a lower deposition, which increases antifouling capacity.

To evaluate the long-term durability of CQACNT-6, normalized PWP and normalized rejection were compared with that of the

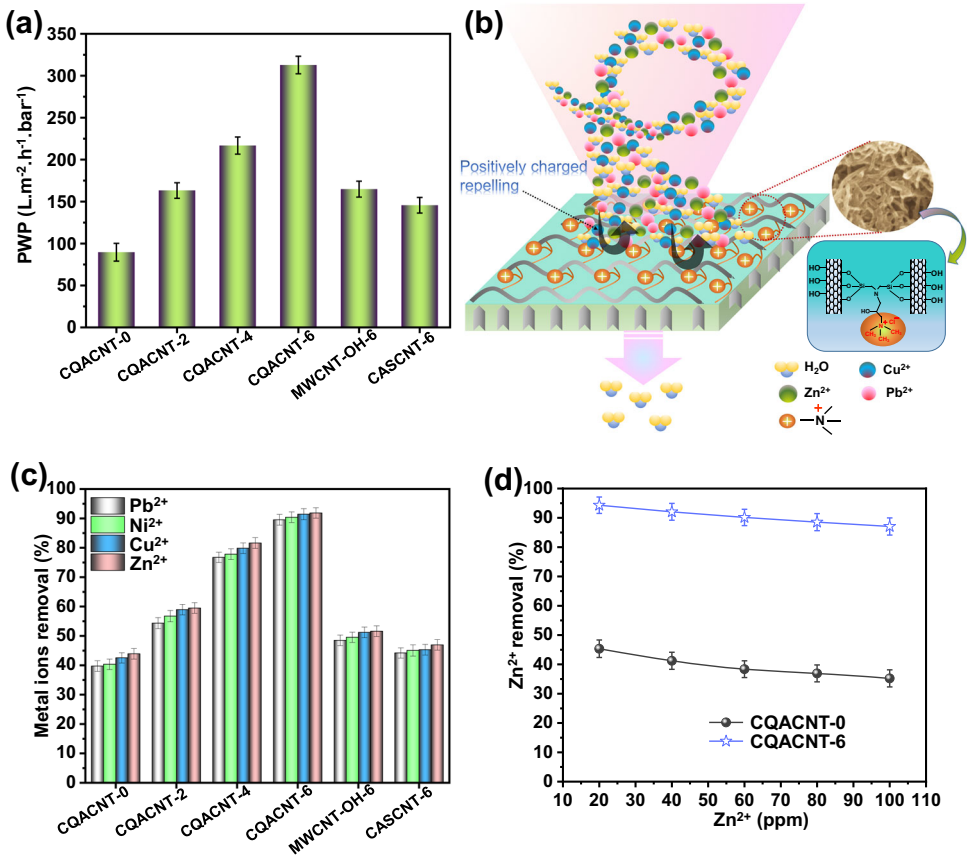

Fig. 8 Comparative performance studies of fabricated membranes. a Pure water permeability; **b** Representation of electrostatic repulsion mechanism between the surface of CQACNT composite membrane and metal ions; **c** Metal ion removal performance of the prepared membranes; **d** Effect of Zn^{2+} concentration on the removal efficiency of CQACNT-0 and CQACNT-6 membranes. Error bars represent the standard deviation between three reported values.

pristine CQACNT-0 membrane using 9- cycles of Cu^{2+} filtration. Deterioration in PWP and rejection of the CQACNT-6 membrane was significantly reduced as compared to the pristine CQACNT-0 membrane (Fig. 9(b)). After 9 filtration cycles, the normalized PWP and rejection efficiency of the CQACNT-6 membrane deteriorated by 13%, and 6%, respectively. This is a significant improvement over the pristine CQACNT-0 membrane, which showed 42%, and 46% deterioration of PWP and rejection, respectively.

Stability of CQACNT in the membrane matrix

The stability of the CQACNT nanomaterial in the developed composite membrane can be attributed to the strong H-bonding between the CQACNT and PES polymer matrix. CQACNT interactions with the PES polymer matrix are schematically represented in Fig. 3(a). The -OH groups of CQACNT interact with the oxygen-containing groups in PES through H-bonding. Furthermore, the stability and interaction of CQACNT within the membrane were confirmed via leaching experiments. A CQACNT-6 membrane coupon was immersed in DI water for 10 d with continuous shaking. The IEC, water contact angle, and FT-IR spectra of the CQACNT-6 membrane showed no significant changes after 10 d and confirmed the stability of CQACNT in the composite membrane (Fig. 10(a)–(c)). The alkaline stability test on the CQACNT-6 composite membrane showed small deterioration in the removal efficiency and PWP after 10 d (Fig. 10(d)). The CQACNT-6 membrane retained 99.1%, 97.27%, and 95.66% of PWP of its initial value after immersion in alkaline solution for 1, 5, and 10 d, respectively. Moreover, the CQACNT-6 membrane retained a removal efficiency of 98.16%, 96.24% and 94.38% of its initial value after immersion in alkaline solution for 1, 5, and 10 d, respectively.

METHODS

Chemicals and materials

Bis[3-(trimethoxysilyl)propyl]amine (BTMSPA, ≥ 90%), poly(vinyl pyrrolidone) (PVP, M_w: 40,000 Da), GTMAC, ethyl alcohol (absolute, ≥99.8%), and N-methyl-2-pyrrolidone (NMP) were purchased from Sigma Aldrich. Poly (ether sulfone) (PES) (M_w: 58,000 g/mol) was purchased from Goodfellow Cambridge Limited, UK. Multiwall carbon nanotubes (−OH) (MWCNT-OH, 98% pure, −OH content ~5.6 wt%) were purchased from mkNANO, Canada. All inorganic salts, including lead nitrate ($Pb(NO_3)_2$), nickel chloride ($NiCl_2$), copper(II) chloride ($CuCl_2$), and zinc chloride ($ZnCl_2$) of analytical grade were purchased from Sigma Aldrich and used without any further purification. Deionized (DI) water (resistivity: 15.1 ± 2.2 MΩ cm, temperature: 23.1 ± 1.5 °C) was used in all experiments.

Synthesis of cross-linked quaternary ammonium carbon nanotube (CQACNT)

Cross-linked quaternary ammonium carbon nanotube (CQACNT) was synthesized in a two-step reaction. The first step involves the silanization of MWCNT-OH by BTMSPA. In a typical synthesis procedure, MWCNT-OH (100 mg) was added to a three-neck round bottom flask with ethyl alcohol (100 mL) and dispersed via ultrasonication for 90 min. Then, BTMSPA (200 µL) was added, and the resulting mixture was left to stir under a nitrogen atmosphere at 70–75 °C for 12 h. The reaction mixture was cooled to room

temperature and ethyl alcohol was removed by filtration using Whatman filter paper (pore size 0.45 µm). Finally, the obtained product was washed with an excess amount of ethyl alcohol and filtered to remove any unreacted BTMSPA molecules. The powder was dried under vacuum for 24 h. The sample was named as cross-linked aminosilane carbon nanotube (CASCNT). The second step involves the epoxide ring-opening reaction of GTMAC. CASCNT (50 mg) and GTMAC (100 µL) were added to a three-neck round bottom flask containing ethyl alcohol (100 mL) and stirred for 3 h at 75 °C. Finally, the reaction mixture was cooled to room temperature, washed with an excess amount of ethyl alcohol, and dried under vacuum for 24 h. Thus, CQACNT was obtained as the final product.

Table 1. Comparison among MWCNT porous membranes reported in the literature and in this work for the removal of toxic metals.

Membrane	PWP (L m^{-2} h^{-1} bar^{-1})	Metal ion	Removal (%)	Reference
PES/ED-MWCNT (0.6 wt%)	8.05	Pb Ni Cu Zn	90.5 90.7 91.9 96.7	14
PEI/PDAMWCNTs/ TMC (M4)	15.32	Cu Zn	90.5 93.0	35
f-CNT	44	Zn	98	36
MWCNTs/chitosan-carrageenan	180	Pb Cu	91 94	37
P-CNT	44	Zn	>98	38
HPEI-MWCNT/PES	75.7	Pb Ni Cu Zn	93.39 94.63 95.84 99.06	39
0.3 wt% of MWCNTs (PCNT-3)	185	Pb	>98	40
CNTs-COOH/CHIT/PS	64.4	Cu Ni Pb Cd Co	71–92.2	41
PEI-grafted-MWCNT-Zn	16.5	Zn	73	12
CQACNT-6	312.8	Pb Ni Cu Zn	89.53 90.42 91.43 91.86	This work

Synthesis of CQACNT composite membranes

The CQACNT composite membranes were prepared by the nonsolvent induced phase separation (NIPS) method. 0–8 wt% of MWCNT-OH, CASCNT and CQACNT relative to PES were dispersed in NMP by bath sonication for 1 h. Then, PVP was gradually added to the above mixture under stirring at room temperature. The PES was then gradually added with constant stirring and the final mixture was kept for 2 h at 70 °C. The subsequent mixture was stirred continuously for another 24 h at room temperature to obtain a homogeneous dope solution. Finally, the doped solution was degassed under a vacuum oven and cast on a glass plate using a casting knife with a thickness of 250 µm. The casted membrane was finally placed in a coagulation bath containing DI water at 24 °C. The prepared membranes were removed from the coagulation bath, washed thoroughly with DI water, and used for characterization. The prepared membranes were named MWCNT-OH-X, CASCNT-X, and CQACNT-X, where X represents the weight percentage of the respective nanomaterial in the composite membrane. The detailed composition of each prepared membrane is given in Supplementary Table 1.

Instrumental characterization of materials and membrane

A series of characterizations were performed for both the material and the membranes. Fourier Transform Infrared Spectroscopy (FT-IR), X-ray Diffraction (XRD), X-ray Photoelectron Spectroscopy (XPS) were applied to study the chemical structure of the synthesized materials and fabricated membranes. Scanning Electron Microscopy (SEM), Transmission electron microscopes (TEM) and Atomic Force Microscope (AFM) were applied to assess the morphology. The measurements of zeta potential, optical images, and water contact angle (WCA; θ) were performed to study the physicochemical properties. The details of all of the above analyses are explained in Supplementary Note 1. The membrane liquid interfacial surface free energy ($-\Delta G_{SL}$) was estimated from modified Young–Dupre equation (Eq. (1)) using the WCA of prepared membranes[32]:

$$-\Delta G_{SL} = \gamma_L\left(1 + \frac{\cos\theta}{1 + SAD}\right) \quad (1)$$

where γ_L is the surface tension of water (72.8 mJ m^{-2}) at 25 °C, and SAD is the difference in surface roughness area. Roughness refers to the ratio of the actual surface area (R_a) to the projected surface area (R_p).

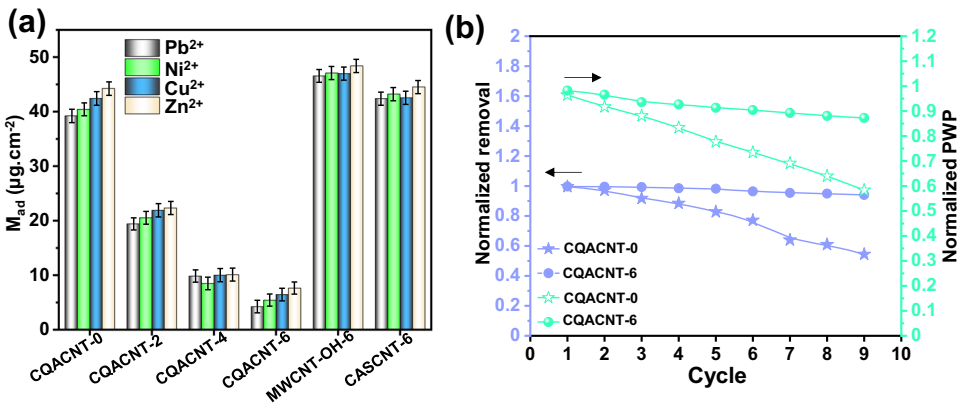

Fig. 9 Adsorption and long-term performance studies of fabricated membranes. a Adsorbed amount of Pb^{2+}, Ni^{2+}, Cu^{2+}, and Zn^{2+} by the developed composite membranes CQACNT, MWCNT-OH-6 and CASCNT-6; **b** Normalized PWP and normalized removal of CQACNT-0 and CQACNT-6 membranes. Error bars represent the standard deviation between three reported values.

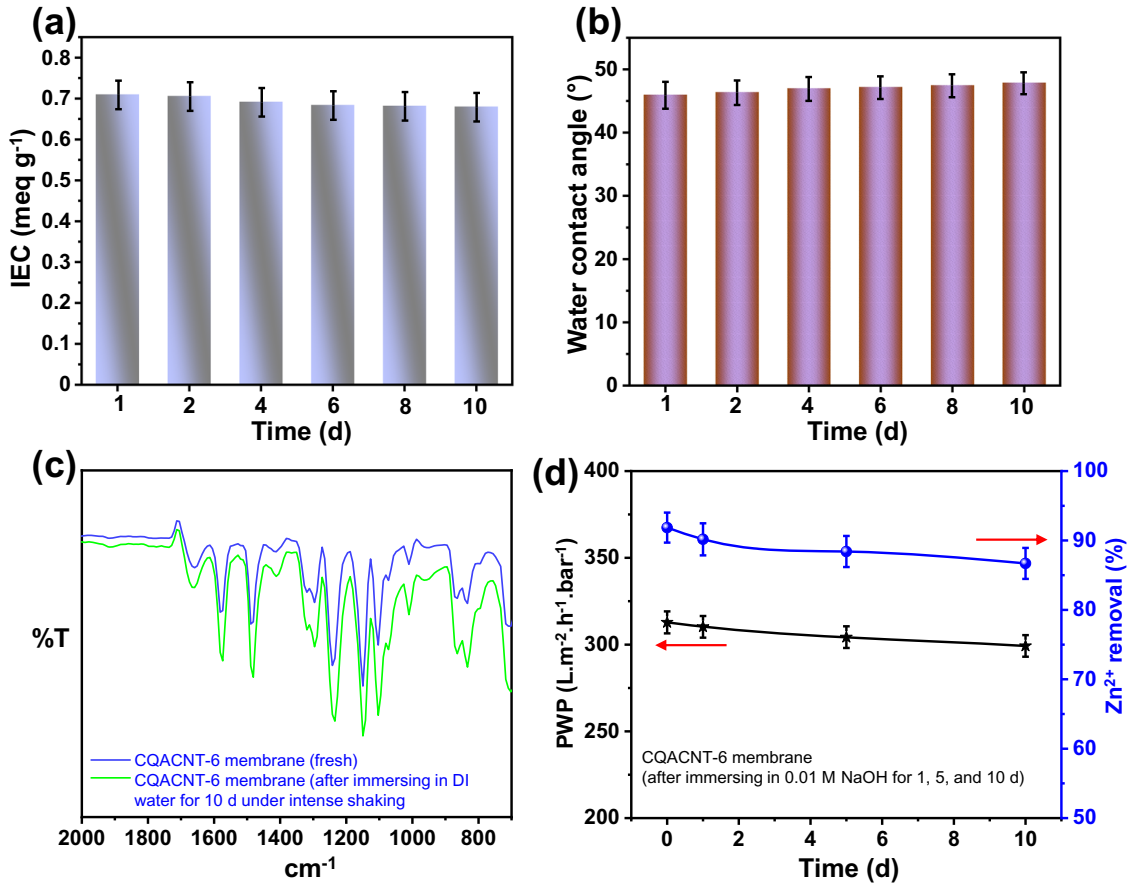

Fig. 10 Evaluation of membrane stability. a IEC of CQACNT-6 composite membrane dipped in DI water for different time intervals (1–10 d); **b** WCA of CQACNT-6 composite membrane dipped in DI water for different time intervals (1–10 d); **c** FT-IR spectra of CQACNT-6 composite membranes; **d** PWP and removal efficiency of CQACNT-6 composite membrane during alkaline stability test for 1, 5, and 10 d. Error bars represent the standard deviation between three reported values.

Water uptake (WU), ion exchange capacity (IEC), porosity, and mean pore size (MPS) measurements of prepared membranes

Detailed methods for estimating water uptake (WU), porosity, and mean pore size (MPS) of prepared membranes are included in Supplementary Note 2 (Supplementary Eq. 1, Supplementary Eq. 2, and Supplementary Eq. 3, respectively). The ion exchange capacity (IEC) of the prepared membranes was determined by the Mohr method, as described in the literature[33]. Briefly, the membranes were dipped into a 1 M NaCl solution for 24 h at 25 °C. The membranes were then removed and thoroughly washed with DI water. Subsequently, the membranes were further dipped into the 0.1 M $NaNO_3$ solution for 24 h at 35 °C, and titrated with 0.01 M $AgNO_3$ solution using K_2CrO_4 indicator to evaluate the Cl^- concentration. The IEC is evaluated using Eq. (2):

$$IEC = N/M_{dry} \tag{2}$$

where N is the milliequivalent amount of the ion exchange group estimated by titration, and M_{dry} is the weight of the dry membrane (g).

Pure water permeability (PWP) and heavy metal ion removal efficiency

The separation performance of the prepared membranes was evaluated by measuring their PWP and metal-ion-removal efficiency. All separation performance experiments were evaluated using a dead-end filtration setup (HP4370 Sterlitech, Co, USA) with an effective membrane area of about 1.25×10^{-3} m^2. The prepared membranes were first compacted by filtering DI water at a pressure of 1.5 bar for 1 h. PWP was calculated using Eq. (3):

$$\mathrm{PWP} = \frac{V}{A\ \Delta t\ \Delta P} \tag{3}$$

where V is the permeate volume of water (L), A is the effective area of the membrane (m^2), Δt is the filtration time (h), and ΔP is the applied pressure (bar).

HM ion retention of the prepared membranes was evaluated by filtering a solution containing a mixture of inorganic salts ($Pb(NO_3)_2$, $NiCl_2$, $CuCl_2$ and $ZnCl_2$) dissolved in DI water with concentration of 45 ppm each salt. A solution of 0.1 M HCl was used to adjust the pH of the prepared solution to ensure solubility and avoid precipitation of HM at high pH. The HM rejection coefficient (R; %) of the prepared membranes was calculated using Eq. (4):

$$R(\%) = \left(1 - \frac{C_p}{C_b}\right) * 100 \tag{4}$$

where C_b and C_p are the concentrations of heavy metal ions in the feed and permeate, respectively. Inductively Coupled Plasma-Optical Emission Spectrometry (ICP-OES; Model 5100 SVDV, Agilent, USA) was used to measure these concentrations.

Antifouling and long-term durability test

The antifouling capacity of the fabricated membranes was evaluated by immersing square membrane coupons (4×4 cm^2) in an aqueous metal salt solution (150 ppm; 50 mL) and kept in a shaker for 24 h. After 24 h, all membranes were removed from the

solution and the amount of metal ions adsorbed by each membrane (M_{ad}) was calculated according to Eq. (5)[34]:

$$M_{ad}\left(\mu g\ cm^{-2}\right) = \frac{(C_i - C_f)V}{A} \quad (5)$$

where C_i, and C_f are the initial and final concentrations (mg L^{-1}) of the metal ion, V is the volume of solution (L), and A is the area of the membrane (cm^2).

Long-term durability was assessed by calculating the flux recovery ratio and rejection recovery ratio in terms of normalized flux and normalized rejection over 9 cycles (each cycle took 2 h). Each cycle begins with the filtration of DI water for 60 min and then salt solution filtration for 60 min. After completion of each cycle, the used membrane was washed with a 0.1 M HCl solution to dissolve any deposited HMs followed by DI water several times. The applied pressure during all experiments was kept constant at 1 bar. Normalized flux and normalized rejection were calculated using Eq. (6) & (7), respectively:

$$\text{Normalized PWP} = \frac{J_f}{J_i} \quad (6)$$

$$\text{Normalized rejection} = \frac{R_f}{R_i} \quad (7)$$

where, J_i, J_f, R_i and R_f are initial PWP, PWP after each cycle, the initial rejection, and the rejection after each cycle of the filtration experiment, respectively.

Stability of CQACNT in the membrane matrix

The stability of CQACNT in the polymer membrane matrix was evaluated by FT-IR, IEC, and WCA investigation of the prepared membrane surface before and after being placed in DI water in a closed vessel for 10 d under vigorous shaking. The alkaline stability of the membrane was tested by dipping the membrane samples in 0.01 M NaOH solution at room temperature for 1, 5, and 10 d. After that, the membranes were washed several times with DI water and the separation performance was evaluated in terms of PWP and rejection.

DATA AVAILABILITY

All data generated or analyzed during this study are included in this published paper, and its supplementary information files.

Received: 12 April 2022; Accepted: 22 August 2022;
Published online: 14 September 2022

REFERENCES

1. Thong, Z. et al. Novel Nanofiltration Membranes Consisting of a Sulfonated Pentablock Copolymer Rejection Layer for Heavy Metal Removal. *Environ. Sci. Technol.* **48**, 13880–13887 (2014).
2. Schwarzenbach, R. P. et al. The Challenge of Micropollutants in Aquatic Systems. *Science* **313**, 1072–1077 (2006).
3. Zou, Y. et al. Environmental Remediation and Application of Nanoscale Zero-Valent Iron and Its Composites for the Removal of Heavy Metal Ions: a Review. *Environ. Sci. Technol.* **50**, 7290–7304 (2016).
4. Li, M. et al. Positively Charged Nanofiltration Membrane with Dendritic Surface for Toxic Element Removal. *ACS Sustain. Chem. Eng.* **5**, 784–792 (2017).
5. Qiu, M. & He, C. Efficient removal of heavy metal ions by forward osmosis membrane with a polydopamine modified zeolitic imidazolate framework incorporated selective layer. *J. Hazard. Mater.* **367**, 339–347 (2019).
6. Nayak, V., Jyothi, M. S., Balakrishna, R. G., Padaki, M. & Deon, S. Novel modified poly vinyl chloride blend membranes for removal of heavy metals from mixed ion feed sample. *J. Hazard. Mater.* **331**, 289–299 (2017).
7. Zhou, M.-Y. et al. A positively charged tight UF membrane and its properties for removing trace metal cations via electrostatic repulsion mechanism. *J. Hazard. Mater.* **373**, 168–175 (2019).
8. Chitpong, N. & Husson, S. M. High-capacity, nanofiber-based ion-exchange membranes for the selective recovery of heavy metals from impaired waters. *Sep. Purif. Technol.* **179**, 94–103 (2017).
9. Hosseini, S. M. et al. A novel layer-by-layer heterogeneous cation exchange membrane for heavy metal ions removal from water. *J. Hazard. Mater.* **381**, 120884 (2020).
10. Pei, X. et al. Robust cellulose-based composite adsorption membrane for heavy metal removal. *J. Hazard. Mater.* **406**, 124746 (2021).
11. Gholami Derami, H. et al. A Robust and Scalable Polydopamine/Bacterial Nanocellulose Hybrid Membrane for Efficient Wastewater Treatment. *ACS Appl. Nano Mater.* **2**, 1092–1101 (2019).
12. Soyekwo, F. et al. Metal in situ surface functionalization of polymer-grafted-carbon nanotube composite membranes for fast efficient nanofiltration. *J. Mater. Chem. A* **5**, 583–592 (2017).
13. Ling, S. et al. Design and function of biomimetic multilayer water purification membranes. *Sci. Adv.* **3**, e1601939 (2017).
14. Peydayesh, M., Mohammadi, T. & Nikouzad, S. K. A positively charged composite loose nanofiltration membrane for water purification from heavy metals. *J. Membr. Sci.* **611**, 118205 (2020).
15. Tian, J., Chang, H., Gao, S. & Zhang, R. How to fabricate a negatively charged NF membrane for heavy metal removal via the interfacial polymerization between PIP and TMC? *Desalination* **491**, 114499 (2020).
16. Wu, B. et al. Chlorine-resistant positively charged polyamide nanofiltration membranes for heavy metal ions removal. *Sep. Purif. Technol.* **275**, 119264 (2021).
17. Tofighy, M. A. & Mohammadi, T. Divalent heavy metal ions removal from contaminated water using positively charged membrane prepared from a new carbon nanomaterial and HPEI. *Chem. Eng. J.* **388**, 124192 (2020).
18. Zheng, J. et al. Facile fabrication of a positively charged nanofiltration membrane for heavy metal and dye removal. *Sep. Purif. Technol.* **282**, 120155 (2022).
19. Gong, X.-Y. et al. Novel high-flux positively charged composite membrane incorporating titanium-based MOFs for heavy metal removal. *Chem. Eng. J.* **398**, 125706 (2020).
20. Li, P. et al. Novel high-flux positively charged aliphatic polyamide nanofiltration membrane for selective removal of heavy metals. *Sep. Purif. Technol.* **280**, 119949 (2022).
21. Macawile, M. C., Quitain, A. T., Kida, T., Tan, R. & Auresenia, J. Green synthesis of sulfonated organosilane functionalized multiwalled carbon nanotubes and its catalytic activity for one-pot conversion of high free fatty acid seed oil to biodiesel. *J. Clean. Prod.* **275**, 123146 (2020).
22. Gaspar, H. et al. Understanding the silylation reaction of multi-walled carbon nanotubes. *Carbon* **49**, 3441–3453 (2011).
23. Shao, L. et al. Multi-walled carbon nanotubes (MWCNTs) functionalized with amino groups by reacting with supercritical ammonia fluids. *Mater. Chem. Phys.* **116**, 323–326 (2009).
24. Siciński, M., Bieliński, D. M., Szymanowski, H., Gozdek, T. & Piątkowska, A. Low-temperature plasma modification of carbon nanofillers for improved performance of advanced rubber composites. *Polym. Bull.* **77**, 1015–1048 (2020).
25. Nasrollahi, N., Aber, S., Vatanpour, V. & Mahmoodi, N. M. Development of hydrophilic microporous PES ultrafiltration membrane containing CuO nanoparticles with improved antifouling and separation performance. *Mater. Chem. Phys.* **222**, 338–350 (2019).
26. Alkhouzaam, A. & Qiblawey, H. Novel polysulfone ultrafiltration membranes incorporating polydopamine functionalized graphene oxide with enhanced flux and fouling resistance. *J. Membr. Sci.* **620**, 118900 (2021).
27. Mayes, A. M., Sivarajan, S. Polymer–Water Interfaces☆, Reference Module in Materials Science and Materials Engineering, Elsevier. https://doi.org/10.1016/B978-0-12-803581-8.03285-9 (2017).
28. Zhu, L. et al. Negatively charged polysulfone membranes with hydrophilicity and antifouling properties based on in situ cross-linked polymerization. *J. Colloid Interfac. Sci.* **498**, 136–143 (2017).
29. Lu, P., Liang, S., Qiu, L., Gao, Y. & Wang, Q. Thin film nanocomposite forward osmosis membranes based on layered double hydroxide nanoparticles blended substrates. *J. Membr. Sci.* **504**, 196–205 (2016).
30. Castro-Muñoz, R., González-Melgoza, L. L. & García-Depraect, O. Ongoing progress on novel nanocomposite membranes for the separation of heavy metals from contaminated water. *Chemosphere* **270**, 129421 (2021).
31. Mu, Y. et al. Fabrication of hybrid ultrafiltration membranes with improved water separation properties by incorporating environmentally friendly taurine modified hydroxyapatite nanotubes. *J. Membr. Sci.* **577**, 274–284 (2019).
32. Huang, T. et al. Improved permeability and antifouling performance of Tröger's base polymer-based ultrafiltration membrane via zwitterionization. *J. Membr. Sci.* **646**, 120251 (2022).
33. Duan, H. et al. Achieving High Conductivity at Low Ion Exchange Capacity for Anion Exchange Membranes with Electrospun Polyelectrolyte Nanofibers. *ACS Appl. Energy Mater.* **3**, 10660–10668 (2020).

34. Ibrahim, Y. et al. Highly selective heavy metal ions membranes combining sulfonated polyethersulfone and self-assembled manganese oxide nanosheets on positively functionalized graphene oxide nanosheets. *Chem. Eng. J.* **428**, 131267 (2022).
35. Zhao, F.-Y. et al. High-Flux Positively Charged Nanocomposite Nanofiltration Membranes Filled with Poly(dopamine) Modified Multiwall Carbon Nanotubes. *ACS Appl. Mater. Interfac.* **8**, 6693–6700 (2016).
36. Ali, S. et al. Efficient removal of zinc from water and wastewater effluents by hydroxylated and carboxylated carbon nanotube membranes: Behaviors and mechanisms of dynamic filtration. *J. Hazard. Mater.* **365**, 64–73 (2019).
37. Alshahrani, A. et al. Enhanced heavy metals removal by a novel carbon nanotubes buckypaper membrane containing a mixture of two biopolymers: Chitosan and i-carrageenan. *Sep. Purif. Technol.* **276**, 119300 (2021).
38. Ali, S., Shah, I. A., Ahmad, A., Nawab, J. & Huang, H. Ar/O2 plasma treatment of carbon nanotube membranes for enhanced removal of zinc from water and wastewater: A dynamic sorption-filtration process. *Sci. Total Environ.* **655**, 1270–1278 (2019).
39. Peydayesh, M., Mohammadi, T. & Bakhtiari, O. Water desalination via novel positively charged hybrid nanofiltration membranes filled with hyperbranched polyethyleneimine modified MWCNT. *J. Ind. Eng. Chem.* **69**, 127–140 (2019).
40. Chandrashekhar Nayak, M. et al. Polyphenylsulfone/multiwalled carbon nanotubes mixed ultrafiltration membranes: Fabrication, characterization and removal of heavy metals Pb2+, Hg2+, and Cd2+ from aqueous solutions. *Arab. J. Chem.* **13**, 4661–4672 (2020).
41. Refaat Alawady, A., Ali Alshahrani, A., Ali Aouak, T. & Mohamed Alandis, N. Polysulfone membranes with CNTs/Chitosan biopolymer nanocomposite as selective layer for remarkable heavy metal ions rejection capacity. *Chem. Eng. J.* **388**, 124267 (2020).

ACKNOWLEDGEMENTS

The authors gratefully acknowledge financial support from Khalifa University of Science and Technology (KU) in Abu Dhabi (UAE) (Award No. CIRA-2020-107). The Center for Membranes and Advanced Water Technology (CMAT) (Award No. RC2-2018-009) KU is also acknowledged.

AUTHOR CONTRIBUTIONS

R.P.: Conceptualization, Methodology, Writing original draft. M.O.: Analysis, Review & Editing. P.A.-R.: Analysis, Review & Editing. F.B.: Review & Editing. S.W.H.: Conceptualization, Validation, Resources, Supervision, Review & Editing, Administration.

COMPETING INTERESTS

The authors declare no competing interests.

ADDITIONAL INFORMATION

Supplementary information The online version contains supplementary material available at https://doi.org/10.1038/s41545-022-00189-8.

Correspondence and requests for materials should be addressed to Shadi W. Hasan.

Reprints and permission information is available at http://www.nature.com/reprints

Publisher's note Springer Nature remains neutral with regard to jurisdictional claims in published maps and institutional affiliations.